A New Shear Locking-Free Quadrilateral Plate Element for Free Vibration and Eigen-Buckling Analysis

Wei XIANG*, Zhixing YAO**, Lina HE***

*School of Mechanical Engineering, Southwest Jiaotong University, China, E-mail: xiangwei@swjtu.edu.cn
**School of Mechanical Engineering, Southwest Jiaotong University, China, E-mail: 813424348@qq.com
***School of Mechanical Engineering, Southwest Jiaotong University, China, E-mail: he20051049@126.com

1. Introduction

In the last few decades, extensive efforts have been devoted to numerical schemes for flexural vibration and eigen-buckling of plates, which are widely used in engineering structures. For the eigenvalue problem of a rectangular geometry, exact or analytical solutions, which often serves as benchmarks for validation of numerical methods, do not always exist except for the special case where at least two parallel edges are simply supported. As for the other boundary conditions, many numerical solutions have been generated by approximate approaches, such as the Rayleigh-Ritz method [1, 2], the differential quadrature method [3, 4], the finite strip [5] and finite element methods [6, 7], etc., among which the finite element method has proven to be very popular, and remains as a focused topic in the research area of computational mechanics [8-12] with growing publication.

It should be pointed out that in early days, most of the research concentrated on the classical plate theory (CPT) which requires displacement and its derivatives to be continuous across element boundaries, thus C^1 continuity is a necessity. However, the neglect of rotary inertia and transverse shear deformation may lead to overestimation of natural frequencies for moderately thick plates.

Efforts, therefore, have been devoted to developing elements based on the Mindlin plate theory (MPT) [13, 14] which accounts for shear deformations, and requires only C^0 continuity for the displacement field. Comparative studies [15-17] have shown that MPT can predict natural frequencies highly consistent with three-dimensional elastic solutions for a variety of plate geometries. But unfortunately, for the finite element approach, formulating a plate bending element based on MPT faces the inevitable difficulty known as the shear locking effect, which arises due to the contradiction between the independence and non-independence among the transverse deflection and two rotations, leading to infinite shear rigidity and unreliable numerical solutions when thick plates are degenerated to thin ones.

In seeking a remedy to the shear locking effect, many researchers have proposed a large number of procedures, among which the reduced and selective reduced integration scheme [18-21] is the most widely used one to correct the locking effect. However, this approach cannot completely eliminate shear locking and it may cause singularity of the stiffness matrix which will often lead to spurious zero-energy modes. Utilizing a mixed formulation based on the multi-variable Hellinger-Reissner principle [22-25] has also proven to be effective in alleviating shear locking, but its practical use might be limited by the difficulty of matching between various field variables and higher requirements

on computing resources due to increased complexity of element formulation.

In recent years, continuous efforts have been made to tackle the aforementioned challenges. Nguyen et al. [26] used a piecewise-linear shape function to derive a polygonal element, in which the assumed strains along the element edges are interpolated based on the Timoshenko's beam formulas so that the shear locking phenomenon can be naturally avoided. Liu et al. [27, 28] proposed the smoothed finite element method (SFEM) by integrating the strain smoothing technique into the classical FEM, and generated various smoothed FEM models which are not only free of shear locking but also insensitive to mesh distortion. Senjanovic et al. [29] gave a shear locking free finite element by decomposing the Mindlin mathematical model of three DOFs into a single-DOF bending model and a double-DOF shear model.

Motivated by the idea of including the shear deformation effect in available thin plate elements [30, 31], the present research proposes a new shear locking-free plate bending element by introducing an extra nodal degree of freedom taking the shear deformation into account on the basis of the classical ACM element [32], following a modified first-order shear deformation theory [33] which only involves two independent variables, namely, the bending deflection w_b and the shearing deflection w_s.

To examine the use of this new developed element in calculating natural frequencies and buckling loads of plates, numerical examples considering various thickness ratios and a range of boundary conditions are presented, and a comprehensive comparison is carried out with available analytical and numerical results in open literature.

2. Modified shear deformation theory

It is widely acknowledged that, CPT can be viewed as an extension of the classical Bernoulli-Euler beam theory (CBT). Likewise, MPT is a two-dimensional equivalent of Timoshenko beam theory (TBT). Both CPT and CBT have one independent variable and one governing equation, however, a Timoshenko beam has two, while MPT has three. Based on this, a two-variable first-order shear deformation theory [33] was developed which decomposes the total deflection into the bending deflection w_b and the shearing deflection w_s, and defines two rotations by the first derivative of w_b. Consider a rectangular plate (length a, width b, uniform thickness h) with its middle surface located in the x-y plane of a Cartesian coordinate system shown in Fig. 1.

The displacement field of this modified first-order plate theory is:

$$u = -z\frac{\partial w_b}{\partial x}, \quad v = -z\frac{\partial w_b}{\partial y}, \quad w = w_b + w_s, \tag{1}$$

where: u, v and w denote the displacements in the x-, y- and z- axes, respectively; w_b and w_s are the deflections caused by the bending and shear deformation, and rotations of a transverse normal with respect to the y- and x- axes are denoted by $\partial w_b/\partial x$ and $\partial w_b/\partial y$, respectively.
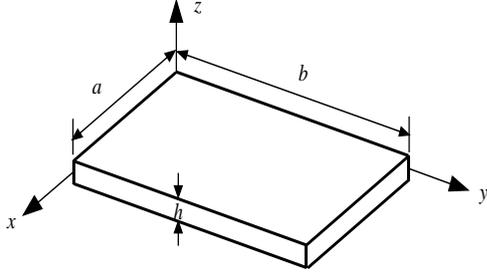
Fig. 1 A rectangular plate and its coordinates

Strains corresponding to the assumed displacement field can be obtained as:

$$\varepsilon_x = \frac{\partial u}{\partial x} = -z\frac{\partial^2 w_b}{\partial x^2}, \quad \varepsilon_y = \frac{\partial v}{\partial y} = -z\frac{\partial^2 w_b}{\partial y^2}$$

$$\gamma_{xy} = \frac{\partial u}{\partial y} + \frac{\partial v}{\partial x} = -2z\frac{\partial^2 w_b}{\partial x \partial y} \tag{2}$$

$$\gamma_{xz} = \frac{\partial u}{\partial z} + \frac{\partial w}{\partial x} = \frac{\partial w_s}{\partial x}, \quad \gamma_{yz} = \frac{\partial v}{\partial z} + \frac{\partial w}{\partial y} = \frac{\partial w_s}{\partial y}$$

These stains can be divided into two groups, one in terms of bending and the other of shearing:

$$\varepsilon_b = \left[\varepsilon_x, \varepsilon_y, \gamma_{xy}\right]^T = -z\left[\frac{\partial^2 w_b}{\partial x^2}, \frac{\partial^2 w_b}{\partial y^2}, 2\frac{\partial^2 w_b}{\partial x \partial y}\right]^T$$

$$\varepsilon_s = \left[\gamma_{xz}, \gamma_{yz}\right]^T = \left[\frac{\partial w_s}{\partial x}, \frac{\partial w_s}{\partial y}\right]^T \tag{3}$$

Similarly, the stress field can be written as:

$$\boldsymbol{\sigma}_b = \left[\sigma_x, \sigma_y, \tau_{xy}\right]^T = \mathbf{D}_b \boldsymbol{\varepsilon}_b, \quad \boldsymbol{\sigma}_s = \left[\tau_{xz}, \tau_{yz}\right]^T = \mathbf{D}_s \boldsymbol{\varepsilon}_s, \tag{4}$$

where the bending and shear rigidity matrices $\mathbf{D}_b$ and $\mathbf{D}_s$ are defined, respectively, as:

$$\mathbf{D}_b = \frac{E}{1-\upsilon^2}\begin{bmatrix} 1 & \upsilon & 0 \\ \upsilon & 1 & 0 \\ 0 & 0 & \frac{1-\upsilon}{2} \end{bmatrix}, \quad \mathbf{D}_s = \begin{bmatrix} \kappa G & \\ & \kappa G \end{bmatrix}, \tag{5}$$

in which υ is the Poisson's ratio; E and $G = E/2(1+\upsilon)$ are Young's modulus and the shear modulus, while κ represents the shear correction factor.

The governing differential equations of motion can be derived from the following Hamilton's principle to guarantee variationally consistency:

$$\delta\Pi = \delta\left(U + V - T\right) = 0, \tag{6}$$

where: Π, U, V and T denote the total potential energy, the strain energy, the potential energy due to external forces and the kinetic energy, respectively, and δ is the symbol of variation.

For free vibration problem, the kinetic and potential energies can be expressed in terms of w_b and w_s as:

$$T = \frac{1}{2}\int_A \rho\left[h\left(\dot{w}_b + \dot{w}_s\right)^2 + J\left(\frac{\partial \dot{w}_b}{\partial x}\right)^2 + J\left(\frac{\partial \dot{w}_b}{\partial y}\right)^2\right]dA,$$

$$U = \frac{1}{2}\int_V \boldsymbol{\varepsilon}_b^T \mathbf{D}_b \boldsymbol{\varepsilon}_b dV + \frac{1}{2}\int_V \boldsymbol{\varepsilon}_s^T \mathbf{D}_s \boldsymbol{\varepsilon}_s dV, \tag{7}$$

where: $J = h^3/12$ is the axial moment of inertia, and ρ is the density of the plate.

Taking w_b and w_s as two independent variables and utilizing the Hamilton's principle, the governing differential equations of motion for free vibrations of the plate can be obtained as:

$$\nabla^2\nabla^2 w_b = -\frac{\rho h}{D}\frac{\partial^2\left(w_b + w_s\right)}{\partial t^2} + \frac{\rho J}{D}\nabla^2\left(\frac{\partial^2 w_b}{\partial t^2}\right),$$

$$\nabla^2 w_s = \frac{\rho h}{S}\frac{\partial^2\left(w_b + w_s\right)}{\partial t^2}, \tag{8}$$

where: $D = Eh^3/12(1-\upsilon^2)$ is the bending rigidity; $S = \kappa Gh$ is the shear rigidity, and ∇^2 is the Laplacian operator.

It can be easily deduced from Eq. (8) that for thin plates where both w_s and J can be taken as zero, the governing equations become:

$$\nabla^2\nabla^2 w_b = -\frac{\rho h}{D}\frac{\partial^2 w_b}{\partial t^2}. \tag{9}$$

Eq. (9) is the same as the governing equation of CPT. Thus the present theory is consistent with CPT, that is, it would reduce to CPT without considering the shearing deflection and rotary inertia.

It needs to be pointed out that in this modified theory, two rotations of the transverse normal are related to the bending deflection, and the shear deformation energy will vanish when a moderately thick plate degenerates to a thin one, thus avoiding the shear locking effect.

The following conclusions can be drawn:

1) This modified two-variable shear deformation plate theory is a two-dimensional equivalent of the Timoshenko beam theory. The extension from the one-dimensional beam theory to its two-dimensional counterpart conforms to unified regularity, i.e., both of them have the same number of independent variables and governing equations.

2) In the present modified theory, the total deflection is composed of the bending and shearing defections, with rotations only related to the bending deflection, and the effect of rotary inertia is involved. In comparison, CPT only considers the bending deflection, and ignores the shearing deflection as well as rotary inertia.

3) In MPT, the rotations ψ_x and ψ_y cannot be determined solely by the deflection w, thus three independent variables exist at the median surface. The present model defines the rotations of the transverse normal by bending slopes $\partial w_b/\partial x$ and $\partial w_b/\partial y$, which conforms to that of the

CPT but violates the hypothesis of MPT. This is a trade-off for a simpler two-variable shear deformation approach versus the more comprehensive hypotheses of MPT involving three variables.

3. Finite element formulation

From Eq. (7), it can be seen that the derivatives with respect to w_b and w_s are of the second and the first order, respectively. Therefore, w_b must be twice differentiable and C^1-continuous, whereas w_s once differentiable and C^0-continuous. And the degrees of freedom required at each node of the element are w_b, $\partial w_b/\partial x$, $\partial w_b/\partial y$ and w_s.

A new four-noded quadrilateral element with 16 degrees of freedom is thus developed to discretize the plate geometry. Dimensionless coordinates ξ and η are introduced as shown in Fig. 2.

$$\xi = \frac{x - x_0}{e_x}, \quad \eta = \frac{y - y_0}{e_y}, \tag{10}$$

where: x_0 and y_0 are the coordinates of the center of the plate in the x-y plane; e_x and e_y are half of the dimensions of the element in the x- and y- axes, respectively.
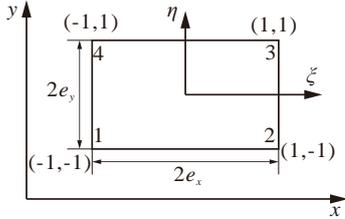
Fig. 2 Dimensionless coordinates of elements

The generalized displacements w_b and w_s are then approximated by using the following interpolation:

$$w_b = \sum_{i=1}^{4} N_i(\xi,\eta)w_{bi} + \sum_{i=1}^{4} N_{xi}(\xi,\eta)\left(\frac{\partial w_b}{\partial y}\right)_i +$$

$$+\sum_{i=1}^{4} N_{yi}(\xi,\eta)\left(\frac{\partial w_b}{\partial x}\right)_i,$$

$$w_s = \sum_{i=1}^{4} M_i(\xi,\eta)w_{si}, \tag{11}$$

where: N_i, N_{xi}, N_{yi} are the shape functions of a non-conforming rectangular thin plate element (ACM element) [32], and M_i the Lagrange interpolation functions, which are also the shape functions of a bilinear quadrilateral four-node (Q4) element [12]. The shape functions are:

$$N_i = \frac{1}{8}(1+\xi_i\xi)(1+\eta_i\eta)(2+\xi_i\xi+\eta_i\eta-\xi^2-\eta^2),$$

$$N_{xi} = -\frac{1}{8}e_y\eta_i(1+\xi_i\xi)(1+\eta_i\eta)(1-\eta^2),$$

$$N_{yi} = \frac{1}{8}e_x\xi_i(1+\xi_i\xi)(1+\eta_i\eta)(1-\xi^2),$$

$$M_i = \frac{1}{4}(1+\xi\xi_i)(1+\eta\eta_i), \quad (i=1,2,3,4). \tag{12}$$

Eq. (11) can be converted into a matrix form:

$$w_b = \mathbf{N}_b\mathbf{d}^e, \quad w_s = \mathbf{N}_s\mathbf{d}^e, \tag{13}$$

in which:

$$\mathbf{N}_b = \left[N_1 \cdots N_4 \ N_{x1} \cdots N_{x4} \ N_{y1} \cdots N_{y4} \ \mathbf{0}_{1\times4}\right]_{1\times16},$$

$$\mathbf{N}_s = \left[0 \ 0 \ \cdots \ 0 \ M_1 \ M_2 \ M_3 \ M_4\right]_{1\times16},$$

$$\mathbf{d}^{eT} = \left[w_{b1} \cdots w_{b4} \ \left(\frac{\partial w_b}{\partial y}\right)_1 \cdots \left(\frac{\partial w_b}{\partial y}\right)_4\right.$$

$$\left.\left(\frac{\partial w_b}{\partial x}\right)_1 \cdots \left(\frac{\partial w_b}{\partial x}\right)_4 \ w_{s1} \cdots w_{s4}\right]_{1\times16}. \tag{14}$$

And the strains can be expressed as:

$$\boldsymbol{\varepsilon}_b = -z\mathbf{B}_b\mathbf{d}^e, \quad \boldsymbol{\varepsilon}_s = \mathbf{B}_s\mathbf{d}^e, \tag{15}$$

in which:

$$\mathbf{B}_b = \left[\frac{\partial^2\mathbf{N}_b}{\partial x^2}; \frac{\partial^2\mathbf{N}_b}{\partial y^2}; 2\frac{\partial^2\mathbf{N}_b}{\partial x\partial y}\right]_{3\times16},$$

$$\mathbf{B}_s = \left[\frac{\partial\mathbf{N}_s}{\partial x}; \frac{\partial\mathbf{N}_s}{\partial y}\right]_{2\times16}. \tag{16}$$

Using the chain rule of differentiation, the derivatives with respect to x and y coordinates can be expressed as:

$$\left[\frac{\partial}{\partial x} \ \frac{\partial}{\partial y}\right]^T = \mathbf{J}_1^{-1}\left[\frac{\partial}{\partial \xi} \ \frac{\partial}{\partial \eta}\right]^T,$$

$$\begin{bmatrix}\dfrac{\partial^2}{\partial x^2}\\[2mm]\dfrac{\partial^2}{\partial y^2}\\[2mm]\dfrac{\partial^2}{\partial x\partial y}\end{bmatrix} = \mathbf{J}_2^{-1}\begin{bmatrix}\dfrac{\partial^2}{\partial \xi^2}\\[2mm]\dfrac{\partial^2}{\partial \eta^2}\\[2mm]\dfrac{\partial^2}{\partial \xi\partial \eta}\end{bmatrix} - \mathbf{J}_2^{-1}\begin{bmatrix}\dfrac{\partial^2 x}{\partial \xi^2} & \dfrac{\partial^2 y}{\partial \xi^2}\\[2mm]\dfrac{\partial^2 x}{\partial \eta^2} & \dfrac{\partial^2 y}{\partial \eta^2}\\[2mm]\dfrac{\partial^2 x}{\partial \xi\partial \eta} & \dfrac{\partial^2 y}{\partial \xi\partial \eta}\end{bmatrix}\mathbf{J}_1^{-1}\begin{bmatrix}\dfrac{\partial}{\partial \xi}\\[2mm]\dfrac{\partial}{\partial \eta}\end{bmatrix}, \tag{17}$$

in which $\mathbf{J}_1$ and $\mathbf{J}_2$ are the first-order and second-order Jacobian matrices as:

$$\mathbf{J} = \begin{bmatrix}\dfrac{\partial x}{\partial \xi} & \dfrac{\partial y}{\partial \xi}\\[2mm]\dfrac{\partial x}{\partial \eta} & \dfrac{\partial y}{\partial \eta}\end{bmatrix}, \quad \mathbf{J} =$$

$$= \begin{bmatrix}\left(\dfrac{\partial x}{\partial \xi}\right) & \left(\dfrac{\partial y}{\partial \xi}\right) & 2\dfrac{\partial x}{\partial \xi}\dfrac{\partial y}{\partial \xi}\\[3mm]\left(\dfrac{\partial x}{\partial \eta}\right) & \left(\dfrac{\partial y}{\partial \eta}\right) & 2\dfrac{\partial x}{\partial \eta}\dfrac{\partial y}{\partial \eta}\\[3mm]\dfrac{\partial x}{\partial \xi}\dfrac{\partial x}{\partial \eta} & \dfrac{\partial y}{\partial \xi}\dfrac{\partial y}{\partial \eta} & \dfrac{\partial x}{\partial \xi}\dfrac{\partial y}{\partial \eta}+\dfrac{\partial x}{\partial \eta}\dfrac{\partial y}{\partial \xi}\end{bmatrix}. \tag{18}$$

Note that the following relation is satisfied:

$$dxdy = |\mathbf{J}|\,d\xi d\eta, \tag{19}$$

where: $|\mathbf{J}_1|$ is the determinant of the Jacobian matrix $\mathbf{J}_1$.

3.1. Free vibration analysis

For free vibration problem, the potential energy due to applied loads equals zero, thus the kinetic energy and the strain energy can be transformed into a simpler form as:

$$U = \frac{1}{2}\mathbf{d}^{eT}\mathbf{K}\mathbf{d}^e, \quad T = \frac{1}{2}\dot{\mathbf{d}}^{eT}\mathbf{M}\dot{\mathbf{d}}^e, \tag{20}$$

in which the stiffness matrix $\mathbf{K}$ and the mass matrix $\mathbf{M}$ are defined as:

$$\mathbf{K} = \frac{h^3}{12}\int_A \mathbf{B}_b^T \mathbf{D}_b \mathbf{B}_b \, dA + h\int_A \mathbf{B}_s^T \mathbf{D}_s \mathbf{B}_s \, dA, \tag{21}$$

$$\mathbf{M} = \int_A \rho \begin{bmatrix} h\left(\mathbf{N}_b + \mathbf{N}_s\right)^T \left(\mathbf{N}_b + \mathbf{N}_s\right) \\ + J\dfrac{\partial \mathbf{N}_b^T}{\partial x}\dfrac{\partial \mathbf{N}_b}{\partial x} + J\dfrac{\partial \mathbf{N}_b^T}{\partial y}\dfrac{\partial \mathbf{N}_b}{\partial y} \end{bmatrix} dA. \tag{22}$$

Applying Eq. (20) into the Hamilton's principle as Eq. (6) leads to the governing equations of free vibrations:

$$\mathbf{M}\ddot{\mathbf{d}}^e + \mathbf{K}\mathbf{d}^e = \mathbf{0}. \tag{23}$$

3.2. Eigen-buckling analysis

Consider a plate subjected to constant initial membrane stress per unit length σ_x^0 in the x- direction, σ_y^0 in the y- direction and a shear stress component τ_{xy}^0 in x-y plane, as shown in Fig. 3.
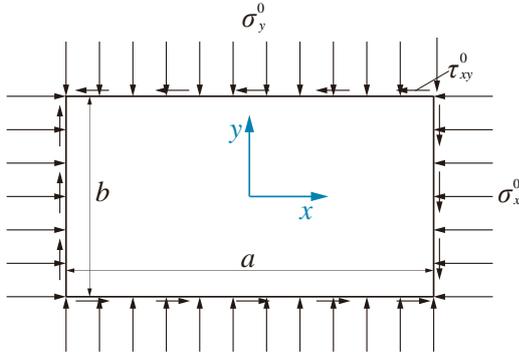
Fig. 3 A rectangular plate subjected to in-plane stresses

For convenience of calculating the critical buckling factors for rectangular plates, the following assumptions are made:

$$\sigma_x^0 \chi_1 = \sigma_{cr}, \quad \sigma_y^0 \chi_2 = \sigma_{cr}, \tag{24}$$

where: χ_1 and χ_2 are the scaling parameters and σ_{cr} is the dimensionless critical buckling load.

Neglecting terms with third and higher-order derivatives, the strain field of the membrane stresses for the assumed displacement field is obtained as:

$$\boldsymbol{\varepsilon}_0 = \begin{bmatrix} \varepsilon_x^0 \\ \varepsilon_y^0 \\ \gamma_{xy}^0 \end{bmatrix} = \frac{1}{2}\begin{bmatrix} \left(\dfrac{\partial u}{\partial x}\right)^2 + \left(\dfrac{\partial v}{\partial x}\right)^2 + \left(\dfrac{\partial w}{\partial x}\right)^2 \\ \left(\dfrac{\partial u}{\partial y}\right)^2 + \left(\dfrac{\partial v}{\partial y}\right)^2 + \left(\dfrac{\partial w}{\partial y}\right)^2 \\ \dfrac{\partial u}{\partial x}\dfrac{\partial u}{\partial y} + \dfrac{\partial v}{\partial x}\dfrac{\partial v}{\partial y} + \dfrac{\partial w}{\partial x}\dfrac{\partial w}{\partial y} \end{bmatrix}. \tag{25}$$

For the eigen-buckling problem, the potential energy V caused by the membrane stresses σ_x^0, σ_y^0 and τ_{xy}^0, can be expressed as the following integration form:

$$V = \int_V \left(\sigma_x^0 \varepsilon_x^0 + \sigma_y^0 \varepsilon_y^0 + 2\tau_{xy}^0 \gamma_{xy}^0\right) dV =$$

$$= \frac{1}{2}\int_A \left[\left(\frac{\partial w}{\partial x} \quad \frac{\partial w}{\partial y}\right)\boldsymbol{\sigma}_0\left(\frac{\partial w}{\partial x} \quad \frac{\partial w}{\partial y}\right)^T\right] h\,dA +$$

$$+ \frac{1}{2}\int_A \left[\left(\frac{\partial^2 w_b}{\partial y\partial x} \quad \frac{\partial^2 w_b}{\partial y^2}\right)\boldsymbol{\sigma}_0\left(\frac{\partial^2 w_b}{\partial y\partial x} \quad \frac{\partial^2 w_b}{\partial y^2}\right)^T\right] \frac{h^3}{12}\,dA +$$

$$+ \frac{1}{2}\int_A \left[\left(\frac{\partial^2 w_b}{\partial x^2} \quad \frac{\partial^2 w_b}{\partial x\partial y}\right)\boldsymbol{\sigma}_0\left(\frac{\partial^2 w_b}{\partial x^2} \quad \frac{\partial^2 w_b}{\partial x\partial y}\right)^T\right] \frac{h^3}{12}\,dA, \tag{26}$$

where:

$$\boldsymbol{\sigma}_0 = \begin{bmatrix} \sigma_x^0 & \tau_{xy}^0 \\ \tau_{xy}^0 & \sigma_y^0 \end{bmatrix}. \tag{27}$$

Define the geometric stiffness matrix $\mathbf{K}_G$ as:

$$\mathbf{K}_G = h\int_A \mathbf{G}_b^T \boldsymbol{\sigma}_0 \mathbf{G}_b \, dA + \frac{h^3}{12}\int_A \left(\mathbf{G}_{s1}^T \boldsymbol{\sigma}_0 \mathbf{G}_{s1} + \mathbf{G}_{s2}^T \boldsymbol{\sigma}_0 \mathbf{G}_{s2}\right) dA, \tag{28}$$

in which:

$$\mathbf{G}_b = \begin{bmatrix} \dfrac{\partial \mathbf{N}_b + \partial \mathbf{N}_s}{\partial x} \\ \dfrac{\partial \mathbf{N}_b + \partial \mathbf{N}_s}{\partial y} \end{bmatrix}, \quad \mathbf{G}_{s1} = \begin{bmatrix} \dfrac{\partial^2 \mathbf{N}_b}{\partial y\partial x} \\ \dfrac{\partial^2 \mathbf{N}_b}{\partial y^2} \end{bmatrix}, \quad \mathbf{G}_{s2} = \begin{bmatrix} \dfrac{\partial^2 \mathbf{N}_b}{\partial x^2} \\ \dfrac{\partial^2 \mathbf{N}_b}{\partial x\partial y} \end{bmatrix}. \tag{29}$$

Utilizing the Hamilton's principle as Eq. (6), the governing equations of the eigen-buckling problem can be expressed as:

$$\left[\mathbf{K} + \lambda\mathbf{K}_G\right]\mathbf{d}^e = \mathbf{0}, \tag{30}$$

where: λ is the buckling factors defined as:

$$\lambda = a^2 h\sigma_{cr}/\pi^2 D. \tag{31}$$

3.3. Boundary conditions

For the present displacement-based finite element formulation, only the displacement boundary conditions need to be strictly satisfied, which are given as:

3.3.1. Simply supported (S)

$$w_b = 0, \quad \frac{\partial w_b}{\partial s} = 0, \; w_s = 0. \tag{32}$$

3.3.2. Clamped (C)

$$w_b = 0, \quad \frac{\partial w_b}{\partial s} = 0, \; \frac{\partial w_b}{\partial n} = 0, \; w_s = 0, \tag{33}$$

where: subscript s and n denote the tangent and the normal of the plate edge, respectively.

It is noteworthy that this new quadrilateral element is established by simply adding one degree of freedom (i.e. the shear deformation w_s) for each node on the basis of the ACM element. This newly developed element takes the effect of shear deformation into account, and does not exhibit shear locking at all, thus is appropriate for both thin and thick plates. Moreover, programming implementation of the new element is simple and efficient, with only minor modification to existing thin plate elements.

4. Numerical results and discussions

The effectiveness of this newly developed element for vibration and eigen-buckling analysis are demonstrated by examples of square plates with edge length a subjected to various boundary constraints. It is noteworthy that though the results presented in this section are for plates of square geometry only, the present element formulation can be readily applied to calculating rectangular plates. Plates are described by a symbolism denoting the corresponding boundary conditions of the four sides. For instance, SCSF implies the following boundary combinations of the four edges: S ($x = 0$) C ($y = 0$) S ($x = a$) F ($y = a$).

4.1. Free vibration analysis

In the following numerical examples, three values of shear correction factor κ (5/6, $\pi^2/12$ and 0.8601) are used to facilitate comparison with corresponding results from other analysis published in open literature. For SSSS plates, κ is taken as 5/6. For CCCC and CCCF plates, $\kappa = 0.8601$. And for SCSC plates, $\kappa = \pi^2/12$. It is found that a limited variation in the value of κ has little effect on the calculated natural frequencies.

A non-dimensional natural frequency is defined as:

$$\bar{\omega} = \omega_{mn} a \sqrt{\rho/G}. \tag{34}$$

where: indices m and n denote the number of half-waves in the x- and y- axes, respectively.

Tables 1 to 4 tabulate the first six natural frequencies of square plates obtained using the new element developed in this study, covering four types of boundary conditions, i.e., SSSS, SCSC, CCCC and CCCF. Analytical or published numerical results are also listed for comparison. All finite element solutions in these tables are generated using mesh of 20×20 elements.

In Tables 1 and 2, comparisons are made between the present solutions and those using Q4 elements [34], as well as the analytical solutions based on MPT [35] for SSSS

and SCSC plates. An overall good agreement can be observed, with the present solutions closer to analytical solutions than those by Q4 elements. Good results of the thin plate verify that the proposed new element does not exhibit the locking effect.

Natural frequencies of CCCC plates are tabulated in Table 3, together with solutions by Q4 elements, the Rayleigh-Ritz method [36] and a meshfree method by Liew [37]. Table 4 compares present results for CCCF plates with the solutions using Q4 elements and a nine-node, quadrilateral Mindlin plate element [38], as well as results by the finite strip method (FSM) [36]. Good agreements are also observed, particularly for thin plates. For the thick geometry, the present method generates solutions slightly higher than Rayleigh-Ritz or FSM solutions for CCCC and CCCF plates, of which analytical solutions do not exist. It can be seen that the newly developed element in the present study imposes more geometrical constraints on the clamped boundary of thick plates, yielding higher natural frequencies for thick plates with clamped boundaries.

Figs. 4 to 6 provide the first four modes of vibration for square plates of different boundary conditions, with thickness ratio $h/a = 0.1$, illustrating the physical patterns of the four modes.

Overall, the results of the present analysis exhibit good accuracy for square plates with different thickness ratios and boundary conditions, confirming the effectiveness of present formulation. Additionally, the present element is very stable and yields no spurious zero-energy modes.

Table 1

Natural frequencies for SSSS plate, $\kappa = 5/6$

Thickness ratio h/a	Number of modes	Present (20×20)	Q4 element (20×20) [34]	Analytical [35]
0.01	1	0.0962	0.0965	0.0963
	2	0.2401	0.2430	0.2406
	3	0.2401	0.2430	0.2406
	4	0.3827	0.3890	0.3847
	5	0.4796	0.4928	0.4807
	6	0.4796	0.4928	0.4807
0.1	1	0.9291	0.9327	0.9303
	2	2.2156	2.2390	2.2193
	3	2.2156	2.2390	2.2193
	4	3.3907	3.4357	3.4056
	5	4.1470	4.2348	4.1494
	6	4.1470	4.2348	4.1494

Table 2

Natural frequencies for SCSC plate, $\kappa = \pi^2/12$

Thickness ratio h/a	Number of modes	Present (20×20)	Q4 element (20×20) [34]	Analytical [35]
0.01	1	0.1409	0.1417	0.1411
	2	0.2659	0.2690	0.2668
	3	0.3370	0.3435	0.3376
	4	0.4576	0.4666	0.4604
	5	0.4961	0.5093	0.4977
	6	0.6266	0.6513	0.6279
0.1	1	1.3224	1.2895	1.3001
	2	2.4211	2.3825	2.3940
	3	2.9497	2.8981	2.8847
	4	3.9144	3.8103	3.8393
	5	4.2554	4.2825	4.2315
	6	5.0207	5.0339	4.9357

Table 3

Natural frequencies for CCCC plate, $\kappa = 0.8601$

Thickness ratio h/a	Number of modes	Present (20×20)	Q4 element (20×20)	Rayleigh-Ritz [36]	Meshfree [37]
0.01	1	0.1750	0.1765	0.1754	0.1743
	2	0.3563	0.3635	0.3576	0.3576
	3	0.3563	0.3635	0.3576	0.3576
	4	0.5227	0.5358	0.5274	0.5240
	5	0.6381	0.6634	0.6402	0.6465
	6	0.6411	0.6666	0.6432	0.6505
0.1	1	1.6043	1.5996	1.5940	1.5582
	2	3.0994	3.0784	3.0390	3.0182
	3	3.0994	3.0784	3.0390	3.0182
	4	4.3587	4.3129	4.2650	4.1711
	5	5.0906	5.1513	5.0350	5.1218
	6	5.1787	5.2011	5.0780	5.1594

Table 4

Natural frequencies for CCCF plate, $\kappa = 0.8601$

Thickness ratio h/a	Number of modes	Present (20×20)	Q4 element (20×20)	Q9 element [38]	FSM [36]
0.01	1	0.1167	0.1174	0.1166	0.1171
	2	0.1946	0.1958	0.1949	0.1951
	3	0.3082	0.3141	0.3082	0.3093
	4	0.3726	0.3787	0.3737	0.3740
	5	0.3912	0.3981	0.3924	0.3931
	6	0.5640	0.5763	0.5678	0.5695
0.1	1	1.0959	1.0870	1.081	1.089
	2	1.8045	1.7506	1.744	1.758
	3	2.7217	2.6989	2.657	2.673
	4	3.2759	3.2309	3.197	3.216
	5	3.4040	3.3248	3.291	3.318
	6	4.7232	4.6025	4.560	4.615

Figs. 7 to 9 show the convergence of the fundamental frequencies for SSSS, CCCC and CCCF plates of both thin ($h/a = 0.01$) and thick ($h/a = 0.1$) geometries in terms of element numbers, and good agreements with analytical solutions [35] and Rayleigh-Ritz solutions [39] are obtained. To measure the error in the finite element solution, we introduce the percentage error with respect to reference values,

$$e = \frac{\omega_{\text{ref}} - \omega}{\omega_{\text{ref}}} \qquad (35)$$

in which ω_{ref} is the analytical solution for SSSS and SCSC plates, and the Rayleigh-Ritz solution for CCCC and CCCF plates, ω denotes the finite element solution.

The percentage errors are also depicted in Figs. 7 to 9. It is shown that the maximum percentage error of present results is less than 1%. Well-behaved convergence characteristics of the present element are demonstrated, and the rate of convergence to the true value is fast and monotonic.

4.2. Eigen-buckling analysis

In this section, a number of numerical examples are carried out to access the new element in buckling analysis of isotropic plates. Four values of shear correction factor κ (0.822, 5/6, $\pi^2/12$ and 0.823045) are used for a proper comparison. Both thin and moderately thick plates with various boundary combinations such as SSSS, SCSC, SCSS, SCSF, SSSF and SFSF are investigated. Different selection of χ_1

and χ_2 are considered, including monoaxial compressive loads in the x ($\chi_1=-1$, $\chi_2=0$) directions, and biaxial compressive loads ($\chi_1=-1$, $\chi_2=-1$).
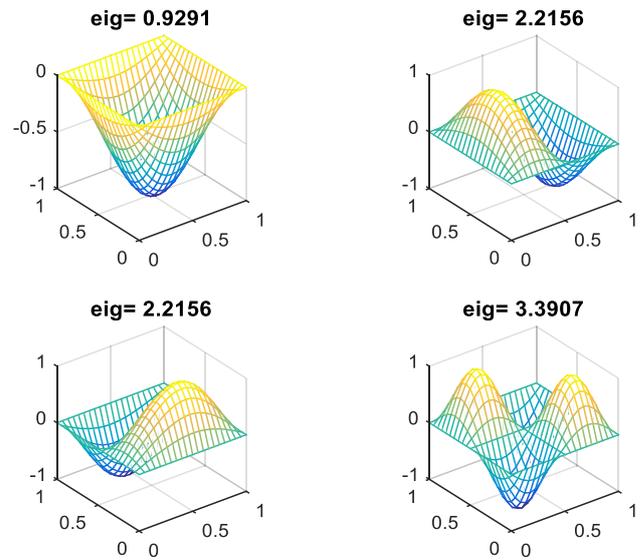
Fig. 4 Modes for SSSS plate ($h/a = 0.1$), mesh 20×20
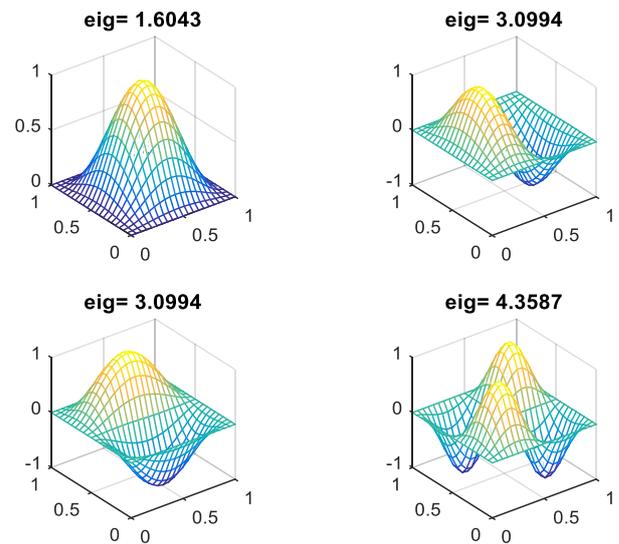
Fig. 5 Modes for CCCC plate ($h/a = 0.1$), mesh 20×20
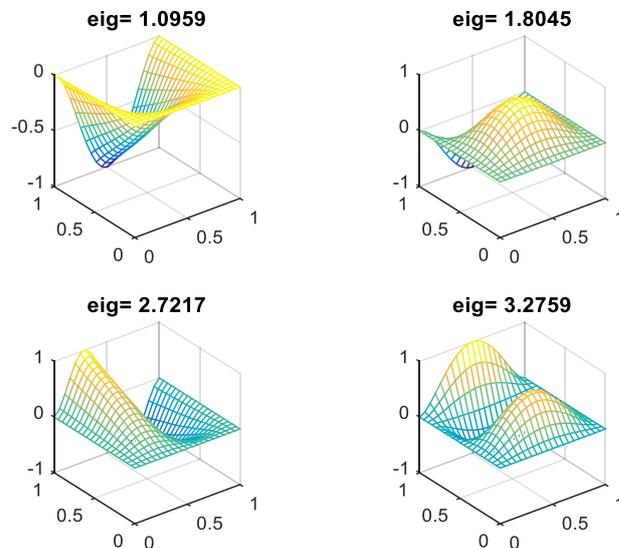
Fig. 6 Modes for CCCF plate ($h/a = 0.1$), mesh 20×20
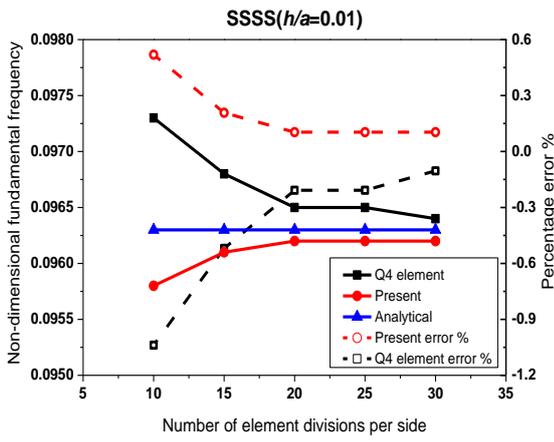
Fig. 7 Convergence of fundamental frequency $\bar{\omega}$ for SSSS plate with $\kappa = 5/6$

Fig. 8 Convergence of fundamental frequency $\bar{\omega}$ for CCCC plate with $\kappa = 0.8601$

Fig. 9 Convergence of fundamental frequency $\bar{\omega}$ for CCCF plate with $\kappa = 0.8601$

Table 5 shows the convergence of the buckling factors for uniaxially loaded ($\chi_1 = -1$, $\chi_2 = 0$) thin square plates ($h/a = 0.01$) with various boundary conditions, and good agreements with analytical solutions [40] are obtained. Well-behaved convergence characteristics of present finite element formulation is clearly demonstrated, and a very good convergence rate for all the considered boundary conditions is shown. It is also shown that for the thin square plate, the ultimate convergence will be to levels slightly lower than the analytical values.

Tables 6 and 7 present the comparisons of the buckling factors with analytical solutions [41], those by Ferreira [34] using Q4 elements, and closed-form solutions by Xing and Xiang [42], for uniaxially and biaxially loaded square plates with thickness ratios $h/b = 0.001$, 0.05, 0.1, and 0.2.

It is observed that a satisfactory agreement between them is achieved, which validates the accuracy of the present element. As expected, the decrease of critical buckling factor is observed with the increase of thickness ratio. This indicates that the shear deformation plays more and more significant roles as a plate gets thicker. Besides, the present results are generally lower than analytical solutions when only simply supported and clamped edges are involved. It is also found that the present results are generally higher than analytical solutions when free edges are involved, and decrease faster than the latter, which indicates that the present formulation weakens the stability of the plate with free edges more intensely as it gets thicker.

Buckling modes for different boundary conditions under uniaxial compression are plotted, see Fig. 10.

Table 5

Convergence of buckling load factor $\lambda=\sigma_{cr}a^2h/\pi^2D$ of square plate ($\chi_1=-1$, $\chi_2=0$, $h/a=0.01$, $\kappa=0.822$)

B.C.	Mesh					Analytical [40]
	10×10	20×20	25×25	30×30	40×40	
SSSS	3.9552	3.9864	3.9903	3.9923	3.9944	4.000
CCCC	9.8582	10.0000	10.0184	10.0286	10.0387	10.070
SCSC	6.6376	6.7078	6.7167	6.7216	6.7265	6.740
CSCS	7.4828	7.6249	7.6429	7.6528	7.6627	7.690
SSSF	1.4336	1.4336	1.4336	1.4336	1.4336	1.440
SCSF	1.6951	1.6969	1.6971	1.6972	1.6973	1.700

Table 6

Buckling factors $\lambda=\sigma_{cr}a^2h/\pi^2D$ for square plate subjected to uniaxial loads ($\chi_1=-1$, $\chi_2=0$, $\kappa=\pi^2/12$)

B.C.	Method	Thickness ratio			
		0.001	0.05	0.1	0.2
SSSS	Present	3.9932	3.9214	3.7231	3.1149
	FEM [34]	4.0141	3.9416	3.7412	3.1273
	Ref. [42]	4	3.9437	3.7838	3.2558
	Analytical	4	3.9437	3.7838	3.2558
SSSC	Present	5.7279	5.5921	5.2249	3.9571
	FEM [34]	5.7693	5.6016	5.1631	3.8934
	Ref. [42]	5.7402	5.6130	5.2644	4.1789
	Analytical [41]	5.7401	5.5977	5.2171	4.1364
SCSC	Present	7.6570	7.2698	6.3332	4.2602
	FEM [34]	7.7580	7.2865	6.2191	4.0733
	Ref. [42]	7.6911	7.3425	6.4705	4.4188
	Analytical [41]	7.6911	7.2989	6.3698	4.3204
SFSF	Present	0.9528	0.9444	0.9203	0.8366
	FEM [34]	0.9549	0.9438	0.9171	0.8294
	Ref. [42]	0.9523	0.9466	0.9300	0.8690
	Analytical [41]	0.9523	0.9431	0.9219	0.8501
SSSF	Present	1.4017	1.3870	1.3450	1.2029
	FEM [34]	1.4048	1.3809	1.3303	1.1756
	Ref. [42]	1.4016	1.3922	1.3647	1.2645
	Analytical [41]	1.4014	1.3813	1.3707	1.2138
SCSF	Present	1.6522	1.6327	1.5770	1.3920
	FEM [34]	1.6559	1.6187	1.5425	1.3251
	Ref. [42]	1.6525	1.6389	1.5993	1.4584
	Analytical [41]	1.6522	1.6197	1.5558	1.3701

Table 7

Buckling factors $\lambda=\sigma_{cr}a^2h/\pi^2D$ for square plate subjected to biaxial loads ($\chi_1=-1$, $\chi_2=-1$)

B.C.	Method	Thickness ratio			
		0.001	0.05	0.1	0.2
SSSS	Present[a]	1.9966	1.9607	1.8616	1.5576
	FEM [34]	2.0070	1.9708	1.8707	1.5639
	Ref. [42]	2	1.9719	1.8920	1.6281
	Analytical	2	1.9718	1.8919	1.7722
SFSF	Present[b]	0.9328	0.9247	0.9013	0.8200
	FEM [34]	0.9348	0.9213	0.8925	0.8026
	Ref. [42]	0.9322	0.9260	0.9080	0.8425
	Analytical	0.9321	0.9207	0.8977	0.8650
SSSF	Present[b]	1.0555	1.0450	1.0147	0.9117
	FEM [34]	1.0581	1.0326	0.9882	0.8642
	Ref. [42]	1.0551	1.0473	1.0247	0.9429
	Analytical	1.0548	1.0322	0.9954	0.9476
SCSF	Present[b]	1.1438	1.1313	1.0957	0.9760
	FEM [34]	1.1465	1.1118	1.0553	0.9070
	Ref. [42]	1.1436	1.1344	1.1078	1.0129
	Analytical	1.1431	1.1119	1.0641	1.0049

[a] shear correction factor $\kappa=0.823045$
[b] shear correction factor $\kappa=5/6$

a) SSSS   b) SSSC

c) SCSC   d) SFSF

e) SSSF   f) SCSF
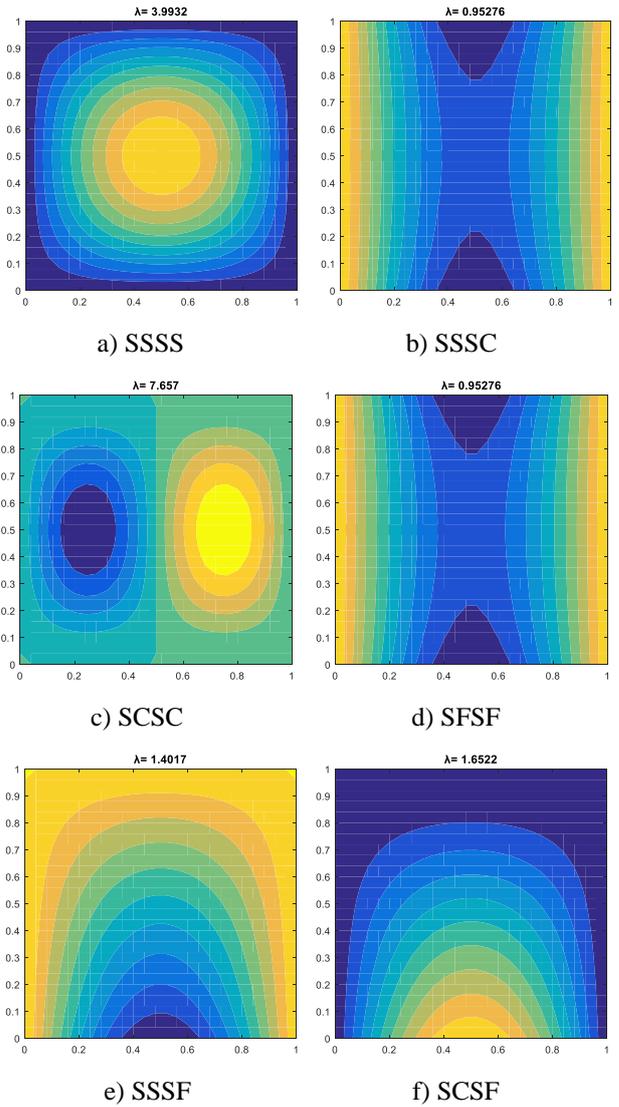
Fig. 10 Buckling modes of square plates under uniaxial compression ($\chi_1=-1$, $\chi_2=0$, $h/a=0.001$)

5. Conclusions

The present newly developed finite element formulation, which is based on a modified first-order shear deformation plate theory, avoids the shear-locking problem seen in other plate elements commonly used. The new formulation reduces to the thin plate theory when the rotary inertia and shearing deflection w_s can be treated as negligible.

Moreover, the present formulation can be easily coded, by including the effect of shear deformations in existing thin plate elements. The model is effective and efficient in programing implementation, requiring only slight modification to existing programing of thin plate elements.

This simple four-noded element for free vibration and eigen-buckling analysis of plates manifests the same or even higher level of accuracy compared with available plate bending elements in literature or some other numerical methods widely acknowledged.

The present research may also be extended to develop more complex elements with more sophisticated geometric shapes and increasing number of nodes, so as to achieve higher level of precision for broader applications.

References

1. **Zhou, D.** 2002. Vibrations of point-supported rectangular plates with variable thickness using a set of static tapered beam functions, International Journal of Mechanical Sciences 44: 149-164.
https://doi.org/10.1016/S0020-7403(01)00081-9.

2. **Zhou, D.; Cheung, Y.; Au, F.; Lo, S.** 2002. Three-dimensional vibration analysis of thick rectangular plates using Chebyshev polynomial and Ritz method, International Journal of Solids and Structures 39: 6339-6353.
https://doi.org/10.1016/S0020-7683(02)00460-2.

3. **Bert, C. W.; Malik, M.** 1996. The differential quadrature method for irregular domains and application to plate vibration, International Journal of Mechanical Sciences 38: 589-606.
https://doi.org/10.1016/S0020-7403(96)80003-8.

4. **Zeng, H.; Bert, C.** 2001. A differential quadrature analysis of vibration for rectangular stiffened plates, Journal of Sound and Vibration 241: 247-252.
https://doi.org/10.1006/jsvi.2000.3295.

5. **Dawe, D.; Wang, S.** 1995. Spline finite strip analysis of the buckling and vibration of rectangular composite laminated plates, International Journal of Mechanical Sciences 37: 645-667.
https://doi.org/10.1016/0020-7403(94)00086-Y.

6. **Putcha, N. S.; Reddy, J. N.** 1986. Stability and natural vibration analysis of laminated plates by using a mixed element based on a refined plate theory, Journal of Sound and Vibration 104: 285-300.
https://doi.org/10.1016/0022-460X(86)90269-5.

7. **Tsay, C. S.; Reddy, J. N.** 1978. Bending, stability and free vibration of thin orthotropic plates by simplified mixed finite elements, Journal of Sound and Vibration 59: 307-311.
https://doi:10.1016/0022-460x(78)90511-4.

8. **Bathe, K.J.** Finite element procedures. (Klaus-Jurgen Bathe, 2006).

9. **Grover ,N.; Singh, B.; Maiti, D.** 2013. Analytical and finite element modeling of laminated composite and sandwich plates: An assessment of a new shear deformation theory for free vibration response, International Journal of Mechanical Sciences 67: 89-99.
https://doi.org/10.1016/j.ijmecsci.2012.12.010.

10. **Talha, M.; Singh, B.** 2010. Static response and free vibration analysis of FGM plates using higher order shear deformation theory, Applied Mathematical Modelling 34: 3991-4011.
https://doi.org/10.1016/j.apm.2010.03.034.

11. **Zhang, B.; Li, H.; Kong, L.; Zhang, X.; Shen, H.** 2020. Strain gradient differential quadrature Kirchhoff plate finite element with the C2 partial compatibility, European Journal of Mechanics-A/Solids 80: 103879.
https://doi.org/10.1016/j.euromechsol.2019.103879.

12. **Zienkiewicz, O. C.; Taylor, R. L.; Nithiarasu, P.; Zhu, J.** 1977. The finite element method. McGraw-hill London, vol. 3.

13. **Mindlin, R. D.** 1951. Influence of Rotatory Inertia and Shear on Flexural Motions of Isotropic, Elastic Plates, Journal of Applied Mechanics 18: 31-38.
https://doi.org/10.1115/1.4010217.

14. **Reissner, E.** 1945. The effect of transverse shear deformation on the bending of elastic plates.
https://doi.org/10.1115/1.4009435.

15. **Iyengar, K. S. R.; Raman, P.** 1977. Free vibration of rectangular plates of arbitrary thickness, Journal of Sound and Vibration 54: 229-236.
https://doi.org/10.1016/0022-460X(77)90025-6.

16. **Srinivas, S.; Rao, C. J.; Rao, A.** 1970. An exact analysis for vibration of simply-supported homogeneous and laminated thick rectangular plates, Journal of Sound and Vibration 12: 187-199.
https://doi.org/10.1016/0022-460X(70)90089-1.

17. **Yu-Chung, L.; Reismann, H.** 1969. Dynamics of rectangular plates, International Journal of Engineering Science 7: 93-113.
https://doi.org/10.1016/0020-7225(69)90025-1.

18. **Hughes, T. J.; Cohen, M.; Haroun, M.** 1978. Reduced and selective integration techniques in the finite element analysis of plates, Nuclear Engineering and Design 46: 203-222.
https://doi.org/10.1016/0029-5493(78)90184-X.

19. **MacNeal, R. H.** 1978. A simple quadrilateral shell element, Computers & Structures 8: 175-183.
https://doi.org/10.1016/0045-7949(78)90020-2.

20. **Pawsey, S. F.; Clough, R. W.** 1971. Improved numerical integration of thick shell finite elements, International Journal for Numerical Methods in Engineering 3: 575-586.
https://doi.org/10.1002/nme.1620030411.

21. **Zienkiewicz, O.; Taylor, R.; Too, J.** 1971. Reduced integration technique in general analysis of plates and shells, International Journal for Numerical Methods in Engineering 3: 275-290.
https://doi.org/10.1002/nme.1620030211.

22. **Auricchio, F.; Taylor, R.** 1995. A triangular thick plate finite element with an exact thin limit, Finite Elements in Analysis and Design 19: 57-68.
https://doi.org/10.1016/0168-874X(94)00057-M.

23. **Kutlu, A.; Omurtag, M. H.** 2012. Large deflection bending analysis of elliptic plates on orthotropic elastic foundation with mixed finite element method, International Journal of Mechanical Sciences 65: 64-74.
https://doi.org/10.1016/j.ijmecsci.2012.09.004.

24. **Lee, S.; Wong, S.** 1982. Mixed formulation finite elements for Mindlin theory plate bending, International Journal for Numerical Methods in Engineering 18: 1297-1311.
https://doi.org/10.1002/nme.1620180903.

25. **Lovadina, C.** 1998. Analysis of a mixed finite element method for the Reissner-Mindlin plate problems, Computer Methods in Applied Mechanics and Engineering 163: 71-85.
https://doi.org/10.1016/S0045-7825(98)00003-6.

26. **Nguyen, N. V.; Nguyen, H. X.; Phan, D. H.; Nguyen-Xuan, H.** 2017. A polygonal finite element method for laminated composite plates, International Journal of Mechanical Sciences 133: 863-882.

https://doi.org/10.1016/j.ijmecsci.2017.09.032.

27. **Liu, G.; Dai, K.; Nguyen, T. T.** 2007. A smoothed finite element method for mechanics problems, Computational Mechanics 39: 859-877. https://doi.org/10.1007/s00466-006-0075-4.

28. **Liu, G.; Nguyen, T.; Dai, K.; Lam, K.** 2007. Theoretical aspects of the smoothed finite element method (SFEM), International Journal for Numerical Methods in Engineering 71: 902-930. https://doi.org/10.1002/nme.1968.

29. **Senjanović, I.; Vladimir, N.; Hadžić, N.** 2014. Modified Mindlin plate theory and shear locking-free finite element formulation, Mechanics Research Communications 55: 95-104. https://doi.org/10.1016/j.mechrescom.2013.10.007

30. **Fricker, A.** 1986. A simple method for including shear deformations in thin plate elements, International Journal for Numerical Methods in Engineering 23: 1355-1366. https://doi.org/10.1002/nme.1620230712.

31. **Yuqiu, L.; Fei, X.** 1992. A universal method for including shear deformation in thin plate elements, International Journal for Numerical Methods in Engineering 34: 171-177. https://doi.org/10.1002/nme.1620340110.

32. **Melosh, R. J.** 1961. A stiffness matrix for the analysis of thin plates in bending, Journal of the Aerospace Sciences 28: 34-42. https://doi.org/10.2514/8.8850.

33. **Xiang, W.; Xing, Y.** 2015. A new first-order shear deformation theory for free vibrations of rectangular plate, International Journal of Applied Mechanics 7: 1550008. https://doi.org/10.1142/S1758825115400086.

34. **Ferreira, A. J.** MATLAB codes for finite element analysis. (Springer, 2009).

35. **Hashemi, S. H.; Arsanjani, M.** 2005. Exact characteristic equations for some of classical boundary conditions of vibrating moderately thick rectangular plates, International Journal of Solids and Structures 42: 819-853. https://doi.org/10.1016/j.ijsolstr.2004.06.063.

36. **Hinton, E.** Numerical methods and software for dynamic analysis of plates and shells. Pineridge Press, 1988.

37. **Liew, K. M.; Wang, J.; Ng, T. Y.; Tan, M. J.** 2004. Free vibration and buckling analyses of shear-deformable plates based on FSDT meshfree method, Journal of Sound and Vibration 276: 997-1017. https://doi.org/10.1016/j.jsv.2003.08.026.

38. **Al Janabi, B. S.; Hinton, E.; Vuksanovic, D.** 1989. Free vibrations of Mindlin plates using the finite element method: Part 1. Square plates with various edge conditions, Engineering Computations. https://doi.org/10.1108/eb023763.

39. **Dawe, D.; Roufaeil, O.** 1980. Rayleigh-Ritz vibration analysis of Mindlin plates, Journal of Sound and Vibration 69: 345-359. https://doi.org/10.1016/0022-460X(80)90477-0.

40. **Timoshenko, S.** Theory of elastic stability 2e. Tata McGraw-Hill Education, 1970.

41. **Hosseini-Hashemi, S.; Khorshidi, K.; Amabili, M.** 2008. Exact solution for linear buckling of rectangular Mindlin plates, Journal of Sound and Vibration 315: 318-342. https://doi.org/10.1016/j.jsv.2008.01.059.

42. **Xing, Y.; Xiang, W.** 2016. Closed-form solutions for eigenbuckling of rectangular Mindlin plate, International Journal of Structural Stability and Dynamics 16: 1550079. https://doi.org/10.1142/S0219455415500790.

W. XIANG, Z.X. YAO, L.N. HE

A NEW SHEAR LOCKING-FREE QUADRILATERAL PLATE ELEMENT FOR FREE VIBRATION AND EIGEN-BUCKLING ANALYSIS

S u m m a r y

A new plate element has been formulated by simply adding one degree of freedom for each node on the basis of the classical ACM element, based on a modified first-order shear deformation plate theory, which assumes that the plate deflection has bending and shearing components, with two rotations defined by differentiations of bending deflections. This new element, with 16 degrees of freedom, exhibits no locking effect, and is appropriate for both thin and thick plates.

To assess the performance of the newly developed plate element, it has been applied to the prediction of natural frequencies and critical bucking loads of square plates with various thickness ratios and boundary conditions. Comparisons with available analytical and numerical solutions in open publication show that the new element leads to highly accurate solutions in free vibration and eigen-buckling analysis with good convergence, and can be competitive with existing plate elements.